AAC Accepted Manuscript Posted Online 5 August 2019
Antimicrob. Agents Chemother. doi:10.1128/AAC.00564-19

Molecular Basis of Class A β-lactamase Inhibition by Relebactam

Catherine L. Tooke[1], Philip Hinchliffe[1], Pauline A. Lang[2], Adrian J. Mulholland[3], Jürgen Brem[2], Christopher J. Schofield[2], and James Spencer[1*].

[1]School of Cellular and Molecular Medicine, Biomedical Sciences Building, University of Bristol, Bristol, BS8 1TD, United Kingdom.

[2]Department of Chemistry, University of Oxford, 12 Mansfield Road, Oxford, OX1 3TA, United Kingdom.

[3]Centre for Computational Chemistry, School of Chemistry, University of Bristol, Cantock's Close, BS8 1TS, Bristol, United Kingdom.

[*]Corresponding author: Jim.Spencer@bristol.ac.uk

Running title: class A β-lactamase inhibition by relebactam

Keywords: serine β-lactamase inhibitors, relebactam, avibactam, diazabicyclooctane, antibiotic resistance.

Abstract

β-Lactamase production is the major β-lactam resistance mechanism in Gram-negative bacteria. β-Lactamase inhibitors (BLIs) efficacious against serine β-lactamase (SBL) producers, especially strains carrying the widely disseminated class A enzymes, are required. Relebactam, a diazabicyclooctane (DBO) BLI is in phase-3 clinical trials in combination with imipenem, for treatment of infections by multi-drug resistant Enterobacteriaceae. We show that relebactam inhibits five clinically-important class A SBLs (despite their differing spectra of activity), representing both chromosomal and plasmid-borne enzymes, i.e. the extended spectrum β-lactamases L2 (inhibition constant 3 μM) and CTX-M-15 (21 μM); and the carbapenemases, KPC-2, -3 and -4 (1 - 5 μM). Against purified class A SBLs, relebactam is an inferior inhibitor compared to the clinically approved DBO avibactam, (9 to 120-fold differences in IC_{50}). Minimum inhibitory concentration assays indicate relebactam potentiates β-lactam (imipenem) activity against KPC-producing *Klebsiella pneumoniae* with similar potency to avibactam (with ceftazidime). Relebactam is less effective than avibactam in combination with aztreonam against *Stenotrophomonas maltophilia* K279a. X-ray crystal structures of relebactam bound to CTX-M-15, L2, KPC-2, KPC-3 and KPC-4 reveal its C2 linked piperidine ring can sterically clash with Asn104 (CTX-M-15) or His/Trp105 (L2 and KPCs), rationalizing its poorer inhibition activity compared to avibactam, which has a smaller C2 carboxyamide group. Mass spectrometry and crystallographic data show slow, pH-dependent relebactam desulfation by KPC-2, -3 and -4. This comprehensive comparison of relebactam binding across five clinically-important class A SBLs will inform the design of future DBOs with the aim of improving clinical efficacy of BLI:β-lactam combinations.

43 **Introduction**

44

45 A major determinant of drug resistance among Gram-negative pathogens is production of β-
46 lactamases, a large enzyme family whose members collectively hydrolyze all β-lactam
47 antibiotics, including cephalosporins and last-resort carbapenems. β-Lactamases are divided
48 into four main classes (A-D) based upon their sequences (1); classes A, C and D are serine-β-
49 lactamases (SBLs), while class B are the zinc-dependent metallo-β-lactamases (MBLs). SBLs
50 hydrolyze antibiotics via formation of a hydrolytically labile 'acyl'-enzyme intermediate,
51 whilst MBL catalysis proceeds without a covalent intermediate (2).

52

53 Of particular clinical importance are the widely disseminated class A SBLs, including the
54 mobile, plasmid-encoded extended-spectrum CTX-M and carbapenem-hydrolyzing KPC
55 families (both produced in opportunistic Gram-negative bacteria such as *Klebsiella*
56 *pneumoniae*, *Pseudomonas aeruginosa*, and *Escherichia coli* (3, 4)), as well as
57 chromosomally-encoded L2 from *Stenotrophomonas maltophilia* (a lung colonist of cystic
58 fibrosis patients, (5, 6)). CTX-M and KPC production significantly threatens current
59 antimicrobial chemotherapy (7, 8). CTX-M-15 is one of the most important members of the
60 CTX-M extended-spectrum β-lactamase (ESBL) family, with a wide spectrum of catalytic
61 activity (3, 8). Of the KPC carbapenemases, KPC-2, KPC-3 and KPC-4 are the most
62 prevalent in resistant Enterobacteriaceae, differing from KPC-2 by single or double point
63 substitutions at positions 104, 240 and 274 (KPC-3 H274Y; KPC-4 P104R/V240G) that
64 change β-lactam specificity, especially toward the oxyimino-cephalosporin ceftazidime (7).
65 L2 (an SBL) is one of two intrinsic β-lactamases, with L1 (an MBL), which together provide
66 resistance to all β-lactams making *S. maltophilia* one of the most extensively drug resistant
67 pathogens in the clinic and one of the most difficult to treat (5).

Three classical β-lactam-based β-lactamase inhibitors (BLIs), i.e. clavulanic acid (9), sulbactam and tazobactam, are used extensively to potentiate β-lactam activity (10). Inhibition is achieved through formation of (an) irreversible, covalent adduct(s) with the catalytic serine of SBLs. These inhibitors have clinically useful (10) potency against class A SBLs, but not typically against enzymes of classes C or D. Since their introduction some class A SBLs have accumulated mutations resulting in inhibitor resistance (11), whilst enzymes such as KPC show reduced susceptibility to inhibition (12). These observations highlight the need for novel BLIs effective against a wider range of β-lactamases.

The diazabicyclooctanes (DBOs), including avibactam (13), relebactam (14), and others (15-17), are a new BLI class with improved activity against a wider range of SBL targets compared to classic BLI scaffolds. Avibactam and relebactam contain the same bicyclic DBO core, differing in their side chains; relebactam contains an additional piperidine ring at C2 (**Figure 1**). DBOs inhibit SBLs through covalent formation of a carbamyl ester to the active-site serine concomitant with DBO ring opening (**Figure 1**). By contrast to clavulanic acid, binding is reversible, with decarbamylation and recyclization observed in CTX-M-15 (18, 19), TEM-1 (13) and KPC-2 (13), as indicated by using 'acyl'-exchange between two serine-β-lactamases. Mass spectrometry of avibactam binding to KPC-2 shows slow hydrolysis over 24 hr, likely following desulfation of the substrate (20). However, under similar conditions relebactam desulfation by KPC-2 was not observed (16), with molecular dynamics suggesting this enhanced relebactam stability results from repositioning of active site water molecules (21, 22).

In 2015 a ceftazidime-avibactam combination (Avycaz/Zavicefa) was approved for the treatment of complicated urinary tract and abdominal infections. This combination expands ceftazidime activity to encompass Gram-negative bacteria producing ESBLs and KPCs. More recently, an imipenem-relebactam combination is in phase-3 clinical trials, restoring the imipenem sensitivity of some resistant *K. pneumoniae* and *P. aeruginosa* (22). However, as with classical BLIs, avibactam resistance is emerging due to mutations/deletions in the β-lactamase target (11, 23); several laboratory generated mutants have provided insight into potential mechanisms for avibactam and likely relebactam resistance (24).

Structural investigations of relebactam are limited to the class C β-lactamase AmpC from *Pseudomonas aeruginosa* at 1.9 Å resolution (PDB 4NK3 (14)). Here, we investigate the structural basis of relebactam inhibition of 5 class A β-lactamases, correlating the results with differences in hydrolytic performance. The ESBLs CTX-M-15 (3) and L2 (25) confer resistance to penicillins, first-, second- and third-generation cephalosporins and the monobactam aztreonam, but are unable to hydrolyze carbapenems; while the hydrolytic capabilities of the KPC carbapenemases (KPC-2, KPC-3 and KPC-4) extend to the potent 'last resort' carbapenems (7, 26). We also provide biochemical and microbiological data to investigate the differences in DBO inhibition across these enzyme families that will inform the design of future inhibitor generations.

Results and Discussion

Relebactam Restores Imipenem Susceptibility of KPC-producing *K. pneumoniae* but is Less Effective Against *S. maltophilia*

The imipenem:relebactam combination (Merck) is currently undergoing phase 3 clinical trials, in particular for treatment of serious infections caused by carbapenem-resistant Enterobacteriaceae (ClinicalTrials.gov identifier: NCT02452047). *In vitro* studies have shown that both the ceftazidime:avibactam and imipenem:relebactam combinations are effective against clinical Enterobacteriacae isolates producing either KPC-2 or KPC-3 (27, 28). However, other KPC variants vary more profoundly in their activities against specific β-lactams (7), whilst relebactam activity against the non-fermenting species *S. maltophilia* is little explored. Accordingly, we compared susceptibilities of recombinant *K. pneumoniae* Ecl8 (29) producing the three most prevalent KPC variants, KPC-2, KPC-3 or KPC-4, to determine efficacy of relebactam combinations against SBL variants with different β-lactam hydrolyzing capabilities, and extended these experiments to include the clinical *S. maltophilia* K279a isolate. *S. maltophilia* causes myriad multi-drug resistant infections, often in immunocompromised patients and is therefore a particularly challenging target for antimicrobial therapy (6). Recently an avibactam:aztreonam combination proved successful in the treatment of several *S. maltophilia* strains (30), we investigate whether this activity is reflected with a relebactam:aztreonam combination.

β-Lactam MICs for KPC variants expressed in *K. pneumoniae* Ecl8 range from 16 mg. L^{-1} to 128 mg. L^{-1} for ceftazidime and 0.5 mg. L^{-1} (KPC-4) to 16 mg. L^{-1} or 64 mg. L^{-1} for imipenem (**Table 1**). This range of MICs is reflected in previously determined k_{cat} values (7) and relative MICs and hydrolysis rates (31) for KPC variants with both substrates. Despite these

differences, imipenem MICs are lowered to ≤0.5 mg. L^{-1} in all KPC producers in the presence of 4 mg. L^{-1} relebactam (**Table 1**), similar to the efficacy of a ceftazidime:avibactam combination. Both combinations can therefore be successful in treating strains producing the range of KPCs (with variable β-lactam hydrolyzing capabilities) in clinical, pathogenic *Enterobacteriaceae*. By way of contrast, the *S. maltophilia* K279a clinical isolate (which produces both L1 (an MBL) and L2 (an SBL)), is resistant to both imipenem and the imipenem:relebactam combination (**Table 1**). We ascribe this to the presence of the L1 MBL, that is able to hydrolyze imipenem and is not inhibited by DBOs (25). However, we, and others (30), have recently demonstrated that several strains of *S. maltophilia* (including K279a) can be inhibited with the monobactam aztreonam (which is not hydrolyzed by L1) combined with a non-classical BL I(25),((30). Indeed, an avibactam/aztreonam combination has been shown to be effective in treating a *S. maltophilia* infection in the clinic (30). Accordingly, we investigated the combination of aztreonam with relebactam against *S. maltophilia* K279a. Addition of relebactam lowers aztreonam MICs from 256 mg. L^{-1} to 8 mg. L^{-1} (**Table 1**), but this compares unfavorably with avibactam, for which aztreonam MICs were lowered to 2 mg. L^{-1} (25). Thus, whilst effective against KPC-producing *K. pneumoniae*, when compared to avibactam, relebactam combinations (in particular with aztreonam) appear to be less effective against *S. maltophilia*.

Relebactam is a Potent Inhibitor of Class A β-Lactamases *in vitro*

Prior kinetic characterization (21) reveals relebactam to be a potent, micromolar, competitive inhibitor of KPC-2. We characterized the inhibition by relebactam, determining values for IC_{50}, K_{iapp} (the apparent dissociation constant for the inhibitory complex as determined from Dixon plots (32)), k_2/K (the apparent second-order rate constant for the onset of carbamylation by relebactam) and k_{off} (rate of recovery of free enzyme), of five class A β-

lactamases, the ESBLs CTX-M-15 and L2 and the carbapenemases KPC-2, KPC-3 and KPC-4 (**Figure 2** and **Figures S1-S4**) and compared these values with those for avibactam. The IC_{50} values (**Table 2**) determined after 10 minutes' pre-incubation with inhibitor indicate that avibactam potently inhibits CTX-M-15 (3.4 nM), with potency decreasing 3-fold for KPC-2 (IC_{50} 10 nM) and KPC-4 (9.3 nM), 5-fold for L2 (15 nM) and 8-fold for KPC-3 (29 nM). Relebactam is substantially less potent than avibactam for each enzyme: by 9-fold (KPC-3), 22-fold (KPC-2), 31-fold (L2), 98-fold (KPC-4) or 119-fold (CTX-M-15). The trends in avibactam and relebactam inhibition across these 5 enzymes are not consistent, for example CTX-M-15 is the most sensitive to avibactam (lowest IC_{50}), but the least sensitive to relebactam (highest IC_{50}, **Table 2**). Importantly, our data indicate that for the tested enzymes relebactam is consistently a substantially inferior inhibitor compared to avibactam (IC_{50} 230 - 910 nM, compared to 3.4 - 29 nM **Table 2**). Furthermore, the > 30-fold increase in IC_{50} between avibactam and relebactam for L2 likely explains the difference in effectiveness of the respective aztreonam combinations against *S. maltophilia* K279a. However, against KPC-expressing *K. pneumoniae*, relebactam combinations are as effective as those with avibactam, suggesting that, in organisms more permeable than *S. maltophilia*, differences in *in vitro* potency between the two DBOs do not translate into effects on MIC for their respective combinations.

More detailed investigation of the time-dependence of relebactam inhibition (**Table 3**) showed that K_{iapp} values, derived from Dixon plots based upon progress curves of initial rates of nitrocefin hydrolysis for enzyme:relebactam mixtures that had not been pre-incubated, generally reflect the IC_{50}, with the exception of CTX-M-15, which has a relatively high K_{iapp} of 21 μM. We consider this high value to reflect the atypically slow carbamylation of the enzyme by relebactam, with a second order rate constant for carbamylation k_2/K of 540

M^{-1} s^{-1} (**Table 3)**. These values are also consistent with others' recent reports of K_{iapp} values for relebactam inhibition of KPC-2 (2.3 μM; (21)) and the Pseudomonas-Derived Cephalosporinase-3 (PDC-3) enzyme (3.4 μM; (33)).

Of the three KPC variants studied, KPC-4 has the highest apparent inhibition constant for relebactam (K_{iapp} 4.8 μM, compared to essentially identical K_{iapp} values for KPC-2 (1.2 μM) and KPC-3 (1.5 μM)). Differences between the three KPC variants are noticeable in their carbamylation rate constants k_2/K; with values for KPC-2 (4500 ± 220 M^{-1} s^{-1}) noticeably faster than for KPC-3 (2100 ± 140 M^{-1} s^{-1}) or KPC-4 (1100 ± 190 M^{-1} s^{-1}). The effect of this is however ameliorated by a reduction of ~4.5 fold in off-rate for both of these variants compared to KPC-2. For L2 (K_{iapp} 2.7 μM) both the second order carbamylation rate constant (4000 ± 620 M^{-1} s^{-1}), and off-rate (0.00055 ± 0.00021s^{-1}) are relatively high. Overall differences in carbamylation rate across the five SBLs tested span almost one order of magnitude, whilst those in off-rate extend to < 5-fold (**Table 3**).

The Structural Basis for Relebactam Inhibition of Class A β-Lactamases

To investigate the molecular basis for relebactam inhibition of class A β-lactamases, and to identify structural explanations for differences in potency, we soaked crystals of CTX-M-15, L2, KPC-2, KPC-3 and KPC-4 with relebactam. For comparison, we also describe crystal structures of native KPC-3 and KPC-4 at 1.22 and 1.42 Å resolution (**Table S3**, **Figures S5A** and **S5B**). Comparison of these structures confirms that, compared to KPC-2, the H274Y and P104R/V240G substitutions do not result in large global conformational changes (**Figure S5C, Table S5**), or induce significant perturbations of the active site (**Figure S5D**).

Relebactam co-complex structures were obtained after 16-hour soaks for CTX-M-15 (1.12 Å, $P2_12_12_1$), L2 (1.78 Å, $P2_12_12_1$), KPC-2 (1.04 Å, $P2_12_12$), KPC-3 (1.06 Å, $P2_12_12$) and KPC-4 (1.04 Å, $P2_12_12$) (**Table S3**). We also obtained a crystal structure for a KPC-4 relebactam complex from data collected after a 1-hour soak. For all of these complex structures there was clear F_o-F_c difference density in the active site into which relebactam could be modelled (**Figure 3**) with ligand real-space correlation coefficients (RSCCs) all greater than 0.93 (**Table S4**). This combination of high resolution and strong difference density enabled us to model the bound inhibitor with a high degree of confidence and enabled us to identify alternative ligand conformations and structures where these were present. For L2, electron density consistent with a single conformation of relebactam (refined at full occupancy) was observed in one of the two molecules in the asymmetric unit (Chain B). Consistent with previous observations for other potent L2 inhibitors in this crystal form we observe a non-covalently bound molecule from the crystallisation solution (D-serine) in the chain A active site(25). In CTX-M-15, relebactam could be refined in two conformations, with occupancies of 0.49 and 0.51. In the KPC variants, structures obtained from diffraction datasets collected after exposing crystals to relebactam for 16 hours were observed to contain both intact and desulfated (i.e. in the imine form) relebactam in the active site, at variable occupancies. For comparison, a KPC-4 structure obtained after the crystal was exposed to inhibitor for just 1 hour revealed only intact relebactam covalently bound in the active site.

Relebactam Interactions with Class A β-Lactamases

Crystal structures of all five class A SBLs tested here reveal relebactam covalently attached to the nucleophilic serine 70 (**Figure 3, Figures S6-S8**). Binding causes no apparent global conformational changes (for comparison, RMSDs between the relevant structures are provided in **Table S5**) and no large changes in any of the active sites compared to those of

the native, un-complexed enzymes. Importantly, the positioning of the 'deacylating' water (Wat1) is apparently little affected by relebactam binding (**Figure 5D, Figures S6-S8**). As seen in previous DBO complex structures (16, 19, 25), relebactam binds as a ring-opened carbamoyl-enzyme complex (13, 14), whereby the six-membered ring adopts a chair conformation (**Figure 3, Figures S6-S8**). The deacylating water, similarly positioned by Glu166 and Asn170 in all complexes, lies close to the C7 atom (see **Figure 1** for atom numbering) of relebactam (2.9Å – 3.2Å), and is apparently positioned for decarbamylation (**Figures S6-S8 panels B and D**). Differences we observe between enzymes in k_{off} (i.e. the decarbamylation rate of the 'acyl'-complex) are therefore probably at least not solemnly due to changes in the position of the deacylating water. A second active site water molecule (Wat2), and its interactions with residues 237 and the N17 atom of relebactam, is also conserved across the 5 enzymes (**Figure 6-8A and D**).

Comparisons of DBO Binding

The efficacy of avibactam and extensive research into structure-activity relationships (SAR) has prompted the development of further generations of DBOs with modifications to the R1 side chain, including relebactam. Comparisons of relebactam binding with other KPC-2, L2 and CTX-M-15 DBO complexes reveal common modes of binding for the inhibitor core. The avibactam carboxyamide side chain in KPC-2 (PDB 4ZBE) adopts a similar geometry to the O16 and N17 atoms of relebactam with the only difference being the position of Wat2 (**Figure S10A**). Despite this movement, Wat2 still hydrogen bonds to the N17 atom in both avibactam and relebactam complexes with KPC-2 (34). WCK-5107, also known as zidebactam, has a K_i against KPC-2 5-fold higher than avibactam and 2-fold higher than relebactam, but only differs from relebactam by an additional amine at position 18. In a KPC-2 complex structure obtained after a 3 hour soak (PDB: 6B1J)(16) (**Figure S10B**) the

piperidine ring of WCK-5107 binds closer (by approximately 3.0 Å) to the backbone oxygen of Cys238 than that of relebactam. The disulfide bond that this residue forms with Cys69 is known to be important to the hydrolytic activity, including carbapenemase activity, of KPC enzymes (35, 36).

In the co-crystal structure of the WCK-5107 complex (**Figure S10C**), a desulfated, imine form of the DBO is modelled, binding similarly to the imine conformation of relebactam observed here. WCK-4234, the most potent DBO described by Papp-Wallace *et al* (16), with cross-class activity against SBLs, binds to KPC-2 with its R1 side chain pointing toward Asn132, in contrast to the N17 of relebactam which points in the 'opposite' direction (**Figure S10D**). As with other DBOs, the N6, O10 and sulfate moiety of WCK-4234 are all flexible, and modelled in a range of different conformations compared with relebactam.

In both CTX-M-15 and L2, DBO binding modes are similar, with only a small rotation of the R1 carboxyamide when comparing avibactam and relebactam (**Figure S10E** and **S10F**). In L2, this results in an additional water molecule, not present in the avibactam complex, that bridges N17 of relebactam (Wat2) with the Ser237 side chain oxygen. For each of the comparisons described above (**Figure S10**), the sulfate moiety and attached O10 atom adopt subtly different conformations in each of the complexes, particularly compared with relebactam. This observation implies flexibility in binding for this region of the DBOs, though numerous factors may underline the differences, including the different resolution limits for each crystal structure, soaking times, or crystallization conditions, and in the case of L2, additional interacting water molecules in the active site.

Hydrogen Bonding of Relebactam in Class A Active Sites

Relebactam is positioned to form hydrogen bonds with the oxyanion hole (Ser70 and Thr237 backbone amides), Asn132 and Ser130, residues that are all conserved (**Figure 4**) in the five enzymes. In the L2 and KPC-variants, the Thr216 backbone oxygen also partakes in hydrogen bond networks (*via* a water molecule, Wat3 in KPCs and Wat3-5 in L2, **Figure 4**), to the relebactam sulfate, an interaction absent in the CTX-M-15 complex. This is probably due to the flexible binding of the sulfate moiety, as described above. In addition, the L2 structure contains two active site water molecules uniquely observed bridging relebactam and residues Tyr272, Arg244, Lys234 and Gly236 (**Figure S6**). These additional interactions in L2 and the KPCs may contribute to the smaller K_i values compared to CTX-M-15 (**Table 3**).

Flexibility in Residues 104 (CTX-M-15) and 105 (L2, KPCs) is Important for Relebactam Binding.

Residues 104 and 105 lie at the entrance of the active site in all class A β-lactamases. Residue 105 has been investigated extensively in TEM-1 (37, 38), SME-1 (35) and KPC-2 (39) and is thought to have important roles in discriminating between, and stabilizing bound, substrates/ intermediates during hydrolysis (**Figure S3**). In the structure of unliganded KPC-2 (PDB 5ul8), Trp105 has poorly defined electron density, suggestive of the presence conformational flexibility (40). Indeed, this is also the case in our unliganded KPC-3 and KPC-4 structures, solved in the same space group ($P2_12_12$), where Trp105 is modelled in two conformations (**Figure S3**). This movement has only been observed in KPC-2 crystal structures solved in the space groups $P2_12_12$ or $P22_12_1$. In other KPC-2 crystal structures solved in different space groups, e.g. 3DW0 (41) and 2OV5 (42), the Trp105-containing loop is stabilized by crystal contacts and Trp105 movement is not observed. In crystal structures of the hydrolysis products of cefotaxime and faropenem non-covalently bound to KPC-2 (40) (space group $P22_12_1$), Trp105 is modelled in one conformation into clear electron density, revealing that

substrate and/or product binding stabilizes the conformation of this residue. However, in the KPC-2:relebactam complex, both Trp105 and the relebactam piperidine ring are modelled in two conformations (**Figure 3**, **Figure 4D** and **Figure S7A**).

In KPC-3 and -4 relebactam complexes Trp105 is modelled in one conformation, similar to one of the two conformations observed in KPC-2, albeit with high B-factors (30.95 and 33.19 compared to average protein B-factors of 13.61 and 13.24, respectively) suggesting there is still flexibility and movement of this residue. In this conformation Trp105 faces the DBO core, with the nitrogen of the pyrrole ring ~3.0 Å from the relebactam imine N6. This is concomitant with well-defined electron density for the relebactam piperidine ring (**Figure 3**). Therefore, movement of Trp105 and binding of the piperidine ring appear linked, with potential for steric clashes to occur if Trp105 were positioned to face the C2 side chain. While the flexibility of this residue may be allowing the KPC-2 active site to accommodate relebactam, the necessity of rearrangement to avoid these steric clashes likely contributes to the decrease in potency of relebactam compared with avibactam.

In the CTX-M-15:relebactam complex, unlike the other SBLs studied here, electron density, for both Asn104 and the relebactam piperidine ring is poorly defined. In crystal structures of wildtype CTX-M enzymes Asn104 is well defined by experimental electron density but is positioned to clash sterically with the expected orientation of the piperidine ring of bound relebactam (**Figure 3 and S9**). Thus, relebactam binding appears to increase the conformational flexibility of CTX-M-15 Asn104 in order to escape such unfavorable interactions. We propose that the need to reposition Asn104 on relebactam binding contributes to the slower carbamylation-rate and higher K_{iapp} (**Table 3**) for CTX-M-15, compared to the other enzymes tested here.

In L2, two conformations of His105 are observed on relebactam binding, with one configuration the same as that observed in the L2:avibactam and native structures, which each contain a single His105 conformation. As in CTX-M-15, these movements are not observed in unliganded enzyme, or in the avibactam-bound L2 structure (25). These energetically unfavorable clashes may indicate why relebactam is 30-fold worse than avibactam at inhibiting L2 (**Table 2**).

With these observations in mind, it is noteworthy that, of DBO compounds tested to date, the compound with the shortest R1-group, WCK-4234, exhibits the greatest potency (K_i) against KPC-2. This may be explained by comparisons of the crystal structures of KPC-2 complexed with WCK-4234 and relebactam (**Figure S10D**); notably, the nitrile R-group of bound WCK-4234 points away from Trp105, whereas the relebactam (piperidine-containing) R-group adopts multiple conformations, of which some clash with Trp105.

Crystal Structures of SBL:Relebactam Complexes Reflect Two Potential Pathways for Relebactam Release

Two pathways for avibactam release (**Figure S11**) are postulated to occur, decarbamylation after DBO recyclization or decarbamylation by direct hydrolysis after loss of the inhibitor sulphate. First, Ehmann *et al* observed, in experiments monitoring transfer of the acylating group between the class A enzymes TEM-1 and CTX-M-15, that decarbamylationoccurs predominantly through regeneration of intact avibactam (i.e. recyclization) (13). Second, in complexes with KPC-2 the avibactam 'acyl'-enzyme can slowly hydrolyze without recyclization, with the observation that only 10% of KPC-2 remains acylated after 24 hours incubation suggestive of a slow, hydrolytic mechanism (20). In time-course experiments

monitoring the stability of the KPC-2:avibactam 'acyl'-enzyme two new 'acyl'-enzyme peaks were identified by MS indicating losses of 79 and 98 Da, consistent with loss of SO_4^{2-} (desulfation) with formation of either hydroxylamine or imine fragments (**Figure S11**). It is thought that these fragmentations precede avibactam loss by hydrolysis and result in relief of inhibition as the released fragments are incapable of forming intact DBO by recyclization.

We therefore examined our various relebactam complex crystal structures with the aim of establishing their compatibility with these competing pathways for loss of covalent attachment from the enzyme. In the CTX-M-15 complex electron density indicates that bound relebactam is in two clear conformations, with occupancies of 0.51 and 0.49 (**Figure 3A**). In one of these two conformations, the relebactam N6 atom interacts closely (2.9 Å) with Ser130, leaving N6 closer to the carbamoyl group than Wat1, and resembling the recyclization 'primed' state previously reported for class A SBLs[12] (PDB:4HBU) (**Figure S6D**). Additionally, short hydrogen bond distances (2.9 Å) are observed between Lys73 and Ser130, similar to those found in the avibactam crystal structure (PDB: 4S2I). Lys73 has been proposed to act as a general base for Ser130 activation for avibactam recyclization(19); the crystal structure of CTX-M-15:relebactam presented here identifies that this is likely also the case for relebactam. This "recyclization primed" conformation for class A enzyme-bound DBOs has only been previously observed in the CTX-M-15:avibactam (19) and the KPC-2:WCK-4234 complexes(16) (**Figure S10**). However, we also note the presence of a second conformation of relebactam in CTX-M-15 that closely resembles that found in avibactam complexes of other enzymes, with N6 positioned further from Ser130 (3.5-4.1 Å) and C7 (**Figure S6, S7 and S8 C+F**) i.e. not primed for recyclization (**Figure S6D, E+F**). The presence of these alternative conformations seems to have little impact on DBO off-rates, with previous studies determining off rates of 1.4 - 6.7 × 10^{-4} s^{-1} for avibactam from CTX-M-

15 (20, 43, 44) and 4.5 ± 0.5 × 10^{-4} s^{-1} for WCK-4234 (16) from KPC-2, similar to the relebactam off-rates observed here (**Table 3**).

In the complex with L2, which contains intact (i.e. non-desulfated, but ring-opened) relebactam in a single conformation, Lys73 and Ser130 were similarly close to one another (**Figure 5**). Despite this proximity, Ser130 is ~ 3.9 Å away from the N6 nitrogen, and so relebactam appears to be still not primed for recyclization in L2. However, in each of the three KPC complexes, in all of which relebactam was a modelled as a mixture of intact and desulfated forms, Lys73 is at least 0.4 Å more distant from Ser130, than is the case for either the CTX-M-15 (either conformation) or L2 structures. These increased distances, when considered with the postulated recyclization pathway that involves proton transfer from Ser130 to Lys73, in addition to the distance of at least 3.5 Å between Ser130 and the N6 of relebactam, suggest that recyclization is less favorable in the KPC complexes than in those formed with the other two enzymes.

Consistent with this possibility, in the KPC-2, KPC-3 and KPC-4 structures, inspection of electron density maps indicated the presence of desulfated relebactam, which could be modelled as the imine form of the inhibitor, with occupancies of 0.35, 0.33 and 0.65 for KPC-2, -3 and -4, respectively. The imine group points towards the flexible Trp105, but otherwise the DBO core closely resembles intact relebactam.

It had previously been thought that relebactam complexes with class A SBLs did not undergo desulfation, with mass spectrometry experiments with KPC-2 suggesting that fragmentation was not occurring even after 24 hours' incubation (16, 21). However, our KPC complex structures provide crystallographic evidence supporting potential relebactam desulfation, at

411 least *in crystallo*, after 16 hours' incubation. To further investigate the possibility of
412 relebactam desulfation, LC-ESI MS studies were carried out on the full-length (codons 25-
413 293) proteins at a range of time points after exposure to both avibactam and relebactam. All
414 KPC variants tested manifested apparently complete carbamylation, without significant
415 fragmentation, by both DBOs within 5 min, in agreement with the fast on-rates we observe
416 kinetically. Initially, acquired spectra showed only adducts of + 265 Da and + 348 Da,
417 respectively, indicating carbamylation of intact avibactam and relebactam, respectively. Over
418 a period of 37 h gradual fragmentation of the complexes to adducts with masses decreased by
419 80 Da and 98 Da (forming the hydroxylamine and imine species, respectively), compared to
420 the initial 'acyl'-enzyme complexes, was observed by the mass spectrometric method
421 employed here. This is in agreement with fragmentation of the initially formed enzyme-
422 inhibitor complexes as described by Ehmann *et al* (13, 20). For all KPC variants tested
423 fragmentation of the avibactam-complex was faster than that of the relebactam-complex, with
424 desulfated avibactam adducts more evident in spectra after 4h incubation and accumulating to
425 higher levels over the duration of the experiment. This slow rate of relebactam desulfation is
426 consistent with the *in crystallo* observations, with relebactam appearing to remain fully
427 sulfated in KPC-4 crystals soaked for 1 hr (**Figure 3C, Figure S8D, E and F**). This complex
428 shows no large differences compared to that obtained after a 16-hour soak (**Figure 3F,**
429 **Figure S8 A, B and C**) with the piperidine ring well defined (**Figure 3C**) and only small
430 changes in the positions of N6, O10 and the sulfate moiety, compared to the other relebactam
431 complexes (**Figure 4**). Additional MS experiments however at pH values ranging from 7.0 –
432 8.5 revealed a significant pH dependence of desulfation, which was enhanced in a basic
433 environment. We note that in crystals soaked in acidic conditions (pH 4-5) no desulfation was
434 observed for other DBOs after 3-hours, yet did occur in longer (~3 days), co-crystallization
435 experiments at the same pH (16).

436

437 These data provide clear evidence that, whilst relebactam:KPC 'acyl'-enzymes can undergo
438 limited desulfation, with the enzymes tested here this occurs much more slowly than for
439 avibactam. It has been previously been suggested, based upon *in silico* docking relebactam
440 into the KPC-2 active site, followed by molecular dynamics simulations, that movements of
441 water molecules away from the sulfate moiety (compared to their positions in avibactam
442 complexes) increase the stability to desulfation of relebactam (21). However, even though we
443 observe a lower rate of relebactam desulfation compared to avibactam, our KPC-2, -3 and -4
444 crystal structures (determined at higher resolution than the previous KPC-2:avibactam
445 complex(34)) all contain an additional active site water molecule (Wat4, **Figure 4**) close to
446 the relebactam sulfate group that is not present in the avibactam complex. Thus, the reason
447 for the increased stability of relebactam, and the mechanism by which the nature of the R1
448 side chain on the DBO core structure affects the desulfation rate, remains uncertain.

449

450 **Conclusions**

451 Diazabicyclooctanes are an emerging and evolving class of BLIs, with the core scaffold
452 capable of accepting modifications at the C2 position that allow further iterations to improve
453 efficacy. Here, we demonstrate that relebactam, the most recent DBO to enter phase 3 clinical
454 trials, inhibits diverse, clinically-relevant class A SBLs: L2, CTX-M-15, and three KPC
455 variants, albeit at reduced potency compared to avibactam. This reduction in potency *in vitro*
456 is not enough to impair the effectiveness of relebactam combinations against relatively
457 permeable *K. pneumoniae* Ecl8 yet does impact efficacy against other organisms. Indeed,
458 compared to the aztreonam:avibactam combination currently being developed for clinical
459 use, an aztreonam:relebactam combination showed decreased efficacy against *S. maltophilia*
460 K279a, indicating likely limitations in the effectiveness of relebactam combinations against

less permeable pathogens. This is consistent with a previous report that relebactam:imipenem combinations are ineffective against *A. baumanii* (14).

Our structural data show unfavorable clashes of the relebactam piperidine ring with β-lactamase residues 104 (CTX-M-15) and 105 (L2 and KPCs) that may explain differences in potency between DBOs. Indeed, the DBO compound WCK-4234, which contains the shortest R1 side chain of those tested to date, displays the greatest potency against class A SBLs, as well as, surprisingly, inhibiting a class D enzyme, OXA-48, with a K_i of 0.29 μM, which compares favorably with values of 30 μM for avibactam and >100 μM for relebactam (16). In addition, DBOs with modifications at the C3 and C4 positions, yet small C2 modifications, also show promising potency across SBL classes, with several compounds, for example ETX2514, exhibiting nanomolar inhibition in IC_{50} assays (17). Our crystal structures also highlight that, compared to avibactam, relebactam makes fewer interactions in the CTX-M-15 complex, which likely contributes to a reduction in potency against this enzyme. Our observations also provide evidence that the relebactam:KPC carbamylated enzyme complex can desulfate, albeit more slowly than that formed with avibactam. These data indicate that the identity of the R1 (C2) side chain of DBOs can influence desulfation, although the underlying mechanism remains to be elucidated. As desulfation prevents recyclization of the inhibitor, leading ultimately to release of inactive degradation products and recovery of active enzyme, this could affect the potency and longevity of the inhibitor. Whilst the timescale of relebactam desulfation that we observe here is noticeably slower than that for avibactam, likely limiting the immediate clinical relevance of this mechanism, its existence raises the possibility that KPC variants capable of supporting faster desulfation may emerge under selection pressure imposed by DBO use. For these reasons the mechanism and determinants of DBO desulfation by different class A β-lactamases deserve more detailed investigation.

The DBO scaffold and current derivations are extremely important additions to the therapeutic arsenal against resistant Gram-negative pathogens. Nevertheless, differences between individual DBOs in potency towards specific enzymes can impact the efficacy of treating problematic β-lactamase producing pathogens, especially "difficult" organisms such as *S. maltophilia*. Our extensive comparisons highlight these differences, and provide significant insights that may guide further development of the core DBO inhibitor scaffold, in particular by emphasising the need to consider the possible impact of C2 substitution on susceptibility of the carbamylated KPC complex to degradation as well as upon interactions with the β-lactamase active site.

Materials and Methods

Minimum Inhibitory Concentration Determination

The pUBYT vector containing *bla*$_{KPC-3}$ under the ISK$_{pn7}$ promoter was used as a template for site-directed mutagenesis to create pUBYT containing *bla*$_{KPC-2}$ and *bla*$_{KPC-4}$ with the same promoter (45). The single point mutation in KPC-2 (Y274H) and double point mutations in KPC-4 (P104R, V240G) were introduced using QuikChange Lightening site-directed mutagenesis kit (Agilent Genomics) with the primers specified in **Table S1**. *Klebsiella pneumoniae* Ecl8 was transformed with the resulting pUBYT constructs via electroporation. *S. maltophilia* K279a is a well-characterized isolate from Bristol, UK, and was obtained as previously reported (46).

MIC values were determined using broth microdilution, in triplicate, in cation-adjusted Mueller Hinton broth (Sigma) according to the Clinical Laboratory Standards Institute (CLSI) guidelines (47). Experiments were performed in microtiter plates (Corning) containing medium with ceftazidime, imipenem or aztreonam with inhibitor (4 mg.L^{-1} avibactam (MedChemExpress) or relebactam (MedChemExpress) dissolved in dimethyl sulfoxide). Plates were incubated overnight at 37 °C for 18–24 h, and the absorbance at 600 nm was read using a POLARstar Omega (BMG LabTech) plate reader.

Protein Purification and Crystallization

The L2 β-lactamase was purified and crystallized as described previously (25). The mature polypeptide (codons 28-290) of CTX-M-15 in the expression vector pOPINF (48) was expressed in SoluBL21 (DE3) *E. coli* cells (Genlantis) and grown in 2xYT medium supplemented with 50 µg/mL carbenicillin to produce N-terminally His-tagged CTX-M-15. 3

litres of culture were incubated at 37°C until reaching an OD_{600} of 0.8 and subsequently grown at 18°C overnight with 0.75 mM IPTG to induce protein expression. Cells were harvested by centrifugation (6,500 × *g*, 10 min) and resuspended in 100 mL of 50 mM HEPES pH 7.5, 400 mM NaCl (Buffer A) with Complete EDTA-free protease inhibitor (Roche), 2 µl Benzonase® Endonuclease and lysozyme (Sigma). Homogenized cells were lysed with 2 passages through a cell disruptor (25 kpsi) and pelleted at 100,000 × *g*, 1 h. Following addition of 10 mM imidazole the supernatant was incubated with 4 mL of Ni-NTA resin (Qiagen) for 1.5 hours. Protein-bound resin was washed in 80 mL of Buffer A plus 10 mM imidazole followed by 40mL of Buffer A plus 20 mM imidazole. Protein was eluted with Buffer A plus 400mM imidazole and concentrated in an Amicon 10-kDa molecular weight cut off (MWCO) centrifugal filter. The imidazole concentration was reduced to 10 mM before addition of 3C protease overnight at 4 °C to remove the N-terminal His-tag. Cleaved tags were captured on Ni-NTA resin following incubation for 1 hour. CTX-M-15 was loaded onto a Superdex S75 column (GE Healthcare) equilibrated with 50mM HEPES 7.5 150mM NaCl and peak fractions analyzed by SDS-PAGE. Fractions assessed as >95% pure were pooled and concentrated to 37 $mg.mL^{-1}$ using an Amicon 10-kDa MWCO centrifugal filter. CTX-M-15 was crystallized using sitting-drop vapor diffusion in CrysChem24 well plates (Hampton Research) at 20°C based on a method previously described (19). Drops comprised 1 µL of protein (15-37 mg/mL) and 1 µL of crystallization reagent (0.1M Tris pH 8.0 and 2.4 M ammonium sulphate) and were equilibrated against 500 µL reagent.

For the KPC variants (KPC-2, KPC-3 and KPC-4) codons 25-293 were cloned into pET28a (Noavagen) and expressed in *E. coli* BL21(DE3) (Novagen). Cells harboring the KPC expression vectors were grown in Auto induction media (Formedium) supplemented with 50

µg/mL kanamycin at 37°C for 8 hours, then at 18°C for 16 hours. Cells were harvested by centrifugation (6,500 × *g*, 10 min), then resuspended in 40 mL of 20 mM Tris pH 8.0, 300 mM NaCl (Buffer B) with a complete EDTA-free protease inhibitor (Roche), 2 µl Benzonase® Endonuclease and lysozyme. Homogenized cells were lysed with 2 passages through a cell disruptor (25 kpsi), then pelleted (100,000 × *g*, 1 h). Following addition of 10 mM imidazole the supernatant was loaded on to a 5 mL His-trap™ column (GE Healthcare) equilibrated with Buffer B. His-tagged protein was eluted by a linear imidazole gradient (20-300 mM) and fractions analyzed by SDS PAGE. Fractions containing KPC were pooled and loaded onto a Superdex S75 column equilibrated with Buffer B and peak fractions analysed by SDS-PAGE. Fractions assessed as >95% pure were pooled and concentrated to 16.3 $mg.mL^{-1}$ KPC-2, 18.2 $mg.mL^{-1}$ KPC-3 and 14.5 $mg.mL^{-1}$ KPC-4 using an Amicon 10-kDa MWCO centrifugal filter.

KPC-2 was crystallized using sitting-drop vapor diffusion in CrysChem24 well plates (Hampton Research) at 20°C based upon previously described conditions (40). Drops comprised 2 µL of protein (16.3 $mg.mL^{-1}$) and 1 µL of crystallisation reagent (2.0 M ammonium sulphate and 5% v/v ethanol) and were equilibrated against 500 µL of reagent. Initial crystals were optimized by seeding with a Seed Bead™ Kit (Hampton research). Drops comprised 2 µL of protein (16.3 $mg.mL^{-1}$), 1 µL crystal seed and 1 µL of crystallisation reagent and were equilibrated against 500 µL reagent. KPC-3 and KPC-4 crystals were grown using the same conditions, using the KPC-2 crystal seed.

Inhibitor Soaking, Data Collection and Structure Determination.

Crystals of L2, CTX-M-15, KPC-2, KPC-3 and KPC-4 were soaked in mother liquor supplemented with 1 mM relebactam. Crystals were then briefly exposed to mother liquor

containing 30% glycerol and flash-frozen in liquid nitrogen. Diffraction data for native and inhibitor-soaked crystals were collected at Diamond Light Source on beamlines I03 (L2 and CTX-M), I04 (KPC-3 and KPC-4) and I24 (KPC-2). Images were indexed and integrated using Dials (49) in the Xia2 (50) pipeline at Diamond Light Source and subsequently scaled in aimless (CCP4 suite (51)). Data were phased by molecular replacement in Phaser (52) (CCP4 suite (51)) with 5NE2 (25) (L2), 4HBT (19) (CTX-M-15) and 5UL8 (40) (KPCs) as the starting structures. Initial refinement in Refmac (53) (CCP4 suite (51)) confirmed F_o-F_c electron density consistent with bound ligand, prior to further rounds of refinement in phenix.refine (54) and manual model building in WinCoot (55). Geometry restrains for relebactam were calculated using eLBOW and omit maps were generated in Phenix (54) from the final model in absence of the ligand. Figures were generated in Pymol (56).

Enzyme Assays.

All enzyme assays were performed at 25 °C in 10 mM HEPES pH 7.5, 150 mM NaCl, with nitrocefin hydrolysis followed at 486 nm (57) ($\Delta\varepsilon$ 486 = 20,500 $M^{-1}.cm^{-1}$) using Greiner half area 96-well plates and a Tecan Infinite 200 Pro microplate reader. Kinetic parameters were calculated and analyzed using GraphPad Prism 6. Steady-state parameters k_{cat} and K_M for nitrocefin hydrolysis were calculated by measuring initial rates of nitrocefin hydrolysis with L2 (1 nM), CTX-M-15 (1 nM), KPC-2 (10 nM), KPC-3 (10 nM) or KPC-4 (10 nM) and plotted against nitrocefin concentration. Steady-state values are provided in **Table S2**.

IC_{50} values were determined by following the initial rates of nitrocefin hydrolysis (50 µM) measured after 10-minute pre-incubation of inhibitor and enzyme (conditions as established by Cahill *et al* (48)). Diazabicyclooctanes were dissolved in DMSO (100 mM) and diluted to the desired concentration in 10 mM HEPES pH 7.5, 150 mM NaCl. Reactions were initiated

by addition of nitrocefin, and initial rates plotted against $\log_{10}$[diazabicyclooctane] and fitted to **Equation 1**. Data were fitted to a four-parameter variable slope to obtain IC_{50} values.

Equation 1.

$$Y=\frac{100}{(1+10^{((LogIC_{50}-[I])*s)})}$$

Y is the observed rate, [I] is inhibitor concentration and s the concentration of substrate (nitrocefin).

The interaction between relebactam (I) and the five enzymes (E) was investigated using kinetic models described previously (**Scheme 1** (13, 17, 20, 43, 58-60)). For DBO inhibitors, interactions with SBLs may be described by two major pathways respectively involving reversible formation of a covalent carbamylated complex (Scheme 1 E-I, whose decarbamylation yields active enzyme and intact inhibitor), and fragmentation of bound inhibitor via desulfation and hydrolysis to liberate active enzyme and non-inhibitory species (20) (**Figure 5**).

$$E + I \underset{k_{-1}}{\overset{k_1}{\rightleftharpoons}} E{:}I \underset{k_{-2}}{\overset{k_2}{\rightleftharpoons}} E - I \xrightarrow{k_3} E - I' \xrightarrow{k_4} E + P$$

Scheme 1:

Formation of the non-covalent (Michaelis) complex E:I is described by the equilibrium constant *K*, equivalent to k_{-1}/k_1 (reverse and forward rate constants, respectively). k_2 is the first-order rate constant for carbamylation, or formation of E-I. k_{-2} is the first-order rate constant for the recyclization step (decarbamylation; reformation of E:I). Formation of

616 covalent imine and desulfated complexes collectively described as E-I' is described by k_3,
617 and release of (inactive) inhibitor degradation product(s) P by k_4.
618
619 Fragmentation of the carbamylated relebactam complex occurs at low levels and was only
620 detected after 4 hours' incubation of enzyme and inhibitor (**Figure 5 C, E and G**).
621 Accordingly, within the time frame of initial velocity experiments described here, **Scheme 1**
622 can be simplified to **Scheme 2** as used to describe slow-binding reversible enzyme inhibition
623 (61).
624 **Scheme 2**:
625
626 $$E + I \underset{k_{-1}}{\overset{k_1}{\rightleftharpoons}} E{:}I \underset{k_{-2}}{\overset{k_2}{\rightleftharpoons}} E - I$$
627 Where k_1 and k_{-1} represent the association and dissociation rate constants for formation of the
628 non-covalent complex described by K, and k_2 and k_{-2} the carbamylation and decarbamylation
629 (recyclization) rate constants, respectively.
630
631 The apparent inhibition constant K_{iapp} (**Scheme 2**; (16, 21, 33, 62-65)) and second-order rate
632 constant for the onset of carbamylation by relebactam k_2/K (see also (13, 17, 20, 43, 58-60))
633 across all enzymes were determined through direct competition assays of relebactam and
634 nitrocefin under steady-state conditions. Nitrocefin was used at a fixed concentration of 50
635 μM; enzyme concentrations used were 1 nM (L2), 2 nM (CTX-M-15) or 10 nM (KPC-2,
636 KPC-3 and KPC-4). K_{iapp}' (uncorrected value for K_{iapp}) was then determined from Dixon
637 plots (32) (of the initial rates (v_0) of nitrocefin hydrolysis (μM/sec) measured in the presence
638 of increasing concentrations of relebactam without pre-incubation. The reciprocals of these
639 initial rates ($1/v_0$) were plotted against relebactam concentration [I], giving a straight line for
640 which the value of the intercept divided by the slope gives K_{iapp}'. These data were corrected

to account for the K_M for nitrocefin ($K_{M(NCF)}$, as determined experimentally, data in **Table S2**) using **Equation 2** to generate values for K_{iapp}**.**

Equation 2.

$$K_{iapp} = K_{iapp}' / 1 + (\frac{[S]}{K_{M(NCF)}})$$

where [S] is the concentration of nitrocefin.

The experiments monitoring nitrocefin hydrolysis in the presence of differing relebactam concentrations were also used to obtain values for k_2/K (apparent second-order rate constant for the onset of carbamylation). Complete progress curves were fitted to **Equation 3** in order to obtain values for k_{obs} (pseudo-first-order rate constant for inactivation).

Equation 3.

$$A = v_f * t + (v_0 - v_f) * ((1 - e^{-k_{obs} * t})/k_{obs}) + A_0$$

Where A is absorbance at 486 nm measured at time t, v_0 and v_f are the initial and final velocities and A_0 the initial absorbance at 486 nm.

The apparent second order rate constant k_2/K was then obtained by plotting k_{obs} against [relebactam] ([I]) according to **Equation 4**, with k_2/K' (uncorrected value for k_2/K) then equal to the slope of the line.

Equation 4.

$$k_{obs} = k_{-2} + k_2/K' * [I]$$

The value obtained for k_2/K' was then corrected using K_M values for nitrocefin ($K_{M(NCF)}$, as determined experimentally, **Table S2**) in **Equation 5** (where [S] is nitrocefin concentration)

to yield k_2/K. (Note that, although the quality of our straight-line fits for k_{obs} against [relebactam] is good, the fact that these experiments (along with others' (21, 33)) necessitated use of relebactam at concentrations approaching K_{iapp} may introduce some uncertainty into values for k_2/K.)

Equation 5.

$$k_2/K = k_2/K' * \left(\left(\frac{[S]}{K_{M(NCF)}}\right) + 1\right)$$

To determine the rate of recovery of free enzyme, k_{off}, 1 µM enzyme was incubated with 17.5 µM relebactam in kinetics buffer (50 mM HEPES pH7.5, 150 mM NaCl) for 10 minutes at room temperature. This mixture was serially diluted and reaction was then assayed by addition of nitrocefin to a final concentration of 50 µM, final enzyme concentrations were as follows: 50 nM KPC-2, 5 nM KPC-3, 50 nM KPC-4, 50 pM CTX-M-15 and 50 pM L2. Complete progress curves were collected, and the results fitted to **Equation 6** to obtain k_{off}.

Equation 6.

$$A = v_f * t + (v_0 - v_f) * (1 - e^{-k_{off} t}) / k_{off} + A_0$$

Where A is absorbance at 486 nm measured at time t, v_0 and v_f are the initial and final velocities and A_0 the initial absorbance at 486 nm.

Mass Spectrometry of Relebactam Fragmentation in KPC Variants.

To investigate modifications to the KPC enzymes by avibactam and relebactam, 3 µM enzyme in 50 mM Tris-HCl pH 7.5 (unless stated otherwise) was incubated with 6 µM avibactam or relebactam at room temperature. Mass spectra were acquired in the positive ion mode using an integrated autosampler/solid phase extraction (SPE) RapidFire365 system

(Agilent Technologies) coupled to an Agilent 6550 Accurate Mass QTOF mass spectrometer. After the indicated time 50 µl of sample was loaded onto a C4 SPE cartridge (Agilent Technologies), washed with buffer D (100% (v/v) water, 0.1% (v/v) formic acid) and subsequently eluted to the mass spectrometer in buffer E (15% (v/v) water, 85% (v/v) acetonitrile, 0.1% (v/v) formic acid). The cartridge was re-equilibrated in buffer D in between samples. Data were analyzed using MassHunter Qualitative Analysis software V.7 (Agilent Technologies) using the maximum entropy deconvolution algorithm.

Acknowledgements

We thank Professor Matthew Avison and Dr Yuiko Takebayashi for the pUBYT-KPC3 plasmid. We also thank the Diamond Light Source for access to beamlines I03, I04 and I24 (Proposal 17212) that contributed to the results presented here and the staff of the Diamond macromolecular crystallography village for their help. In addition, this work has been facilitated by the BrisSynBio Biosuite (UK Biotechnology and Biological Sciences (BBSRC) and Engineering and Physical Sciences (EPSRC) Research Councils, BB/L01386X/1) and the BBSRC ALERT14 equipment initiative (BB/M012107/1). Research was supported by the BBSRC-funded South West Biosciences Doctoral Training Partnership (training grant reference BB/J014400/1, studentship to CLT). Support has also been received from the EPSRC (EP/M022609/1 and EP/M013219/1; AJM) and UK Medical Research Foundation (MRF-145-0004-TPG-AVISO; PAL and CJS). JB and CJS acknowledge support from the Wellcome Trust and the Innovative Medicines Initiative Joint Undertaking under grant agreement no 115583 resources of which are composed of financial contributions from the European Union`s Seventh Framework Programme (FP7/2007-2013) and EFPIA companies` in kind contribution. JS has received research funding from Allecra Therapeutics. We thank Gary Dmitrienko and Malcolm Page for their comments on the manuscript and for discussions.

716 **References**

717 1. Ambler RP, Coulson AF, Frère JM, Ghuysen JM, Joris B, Forsman M, Levesque RC,
718 Tiraby G, Waley SG. 1991. A standard numbering scheme for the class A beta-
719 lactamases. Biochem J 276 (Pt 1):269-70.

720 2. Bush K, Jacoby GA. 2010. Updated functional classification of beta-lactamases.
721 Antimicrob Agents Chemother 54:969-76.

722 3. Cantón R, González-Alba JM, Galán JC. 2012. CTX-M Enzymes: Origin and
723 Diffusion. Front Microbiol 3:110.

724 4. Arnold RS, Thom KA, Sharma S, Phillips M, Kristie Johnson J, Morgan DJ. 2011.
725 Emergence of Klebsiella pneumoniae carbapenemase-producing bacteria. South Med
726 J 104:40-5.

727 5. Calvopiña K, Umland KD, Rydzik AM, Hinchliffe P, Brem J, Spencer J, Schofield
728 CJ, Avison MB. 2016. Sideromimic Modification of Lactivicin Dramatically
729 Increases Potency against Extensively Drug-Resistant Stenotrophomonas maltophilia
730 Clinical Isolates. Antimicrob Agents Chemother 60:4170-5.

731 6. Abbott IJ, Peleg AY. 2015. Stenotrophomonas, Achromobacter, and nonmelioid
732 Burkholderia species: antimicrobial resistance and therapeutic strategies. Semin
733 Respir Crit Care Med 36:99-110.

734 7. Mehta SC, Rice K, Palzkill T. 2015. Natural Variants of the KPC-2 Carbapenemase
735 have Evolved Increased Catalytic Efficiency for Ceftazidime Hydrolysis at the Cost
736 of Enzyme Stability. PLoS Pathog 11:e1004949.

737 8. Bonnet R. 2004. Growing group of extended-spectrum beta-lactamases: the CTX-M
738 enzymes. Antimicrob Agents Chemother 48:1-14.

739 9. Fritz RA, Alzate-Morales JH, Spencer J, Mulholland AJ, van der Kamp MW. 2018.
740 Multiscale Simulations of Clavulanate Inhibition Identify the Reactive Complex in

Class A β-Lactamases and Predict the Efficiency of Inhibition. Biochemistry 57:3560-3563.

10. Drawz SM, Bonomo RA. 2010. Three decades of beta-lactamase inhibitors. Clin Microbiol Rev 23:160-201.

11. Papp-Wallace KM, Bonomo RA. 2016. New β-Lactamase Inhibitors in the Clinic. Infect Dis Clin North Am 30:441-464.

12. Papp-Wallace KM, Bethel CR, Distler AM, Kasuboski C, Taracila M, Bonomo RA. 2010. Inhibitor resistance in the KPC-2 beta-lactamase, a preeminent property of this class A beta-lactamase. Antimicrob Agents Chemother 54:890-7.

13. Ehmann DE, Jahić H, Ross PL, Gu RF, Hu J, Kern G, Walkup GK, Fisher SL. 2012. Avibactam is a covalent, reversible, non-β-lactam β-lactamase inhibitor. Proc Natl Acad Sci U S A 109:11663-8.

14. Blizzard TA, Chen H, Kim S, Wu J, Bodner R, Gude C, Imbriglio J, Young K, Park YW, Ogawa A, Raghoobar S, Hairston N, Painter RE, Wisniewski D, Scapin G, Fitzgerald P, Sharma N, Lu J, Ha S, Hermes J, Hammond ML. 2014. Discovery of MK-7655, a β-lactamase inhibitor for combination with Primaxin®. Bioorg Med Chem Lett 24:780-5.

15. Bush K, Bradford PA. 2019. Interplay between β-lactamases and new β-lactamase inhibitors. Nat Rev Microbiol 17:295-306.

16. Papp-Wallace KM, Nguyen NQ, Jacobs MR, Bethel CR, Barnes MD, Kumar V, Bajaksouzian S, Rudin SD, Rather PN, Bhavsar S, Ravikumar T, Deshpande PK, Patil V, Yeole R, Bhagwat SS, Patel MV, van den Akker F, Bonomo RA. 2018. Strategic Approaches to Overcome Resistance against Gram-Negative Pathogens Using β-Lactamase Inhibitors and β-Lactam Enhancers: Activity of Three Novel

765 Diazabicyclooctanes WCK 5153, Zidebactam (WCK 5107), and WCK 4234. J Med
766 Chem 61:4067-4086.
767 17. Durand-Réville TF, Guler S, Comita-Prevoir J, Chen B, Bifulco N, Huynh H, Lahiri
768 S, Shapiro AB, McLeod SM, Carter NM, Moussa SH, Velez-Vega C, Olivier NB,
769 McLaughlin R, Gao N, Thresher J, Palmer T, Andrews B, Giacobbe RA, Newman JV,
770 Ehmann DE, de Jonge B, O'Donnell J, Mueller JP, Tommasi RA, Miller AA. 2017.
771 ETX2514 is a broad-spectrum β-lactamase inhibitor for the treatment of drug-resistant
772 Gram-negative bacteria including Acinetobacter baumannii. Nat Microbiol 2:17104.
773 18. Choi H, Paton RS, Park H, Schofield CJ. 2016. Investigations on recyclisation and
774 hydrolysis in avibactam mediated serine β-lactamase inhibition. Org Biomol Chem
775 14:4116-28.
776 19. Lahiri SD, Mangani S, Durand-Reville T, Benvenuti M, De Luca F, Sanyal G,
777 Docquier JD. 2013. Structural insight into potent broad-spectrum inhibition with
778 reversible recyclization mechanism: avibactam in complex with CTX-M-15 and
779 Pseudomonas aeruginosa AmpC β-lactamases. Antimicrob Agents Chemother
780 57:2496-505.
781 20. Ehmann DE, Jahic H, Ross PL, Gu RF, Hu J, Durand-Réville TF, Lahiri S, Thresher
782 J, Livchak S, Gao N, Palmer T, Walkup GK, Fisher SL. 2013. Kinetics of avibactam
783 inhibition against Class A, C, and D β-lactamases. J Biol Chem 288:27960-71.
784 21. Papp-Wallace KM, Barnes MD, Alsop J, Taracila MA, Bethel CR, Becka SA, van
785 Duin D, Kreiswirth BN, Kaye KS, Bonomo RA. 2018. Relebactam Is a Potent
786 Inhibitor of the KPC-2 β-Lactamase and Restores Imipenem Susceptibility in KPC-
787 Producing Enterobacteriaceae. Antimicrob Agents Chemother 62:e00174-18.
788 22. Zhanel GG, Lawrence CK, Adam H, Schweizer F, Zelenitsky S, Zhanel M, Lagacé-
789 Wiens PRS, Walkty A, Denisuik A, Golden A, Gin AS, Hoban DJ, Lynch JP,

Karlowsky JA. 2018. Imipenem-Relebactam and Meropenem-Vaborbactam: Two Novel Carbapenem-β-Lactamase Inhibitor Combinations. Drugs 78:65-98.

23. Hemarajata P, Humphries RM. 2019. Ceftazidime/avibactam resistance associated with L169P mutation in the omega loop of KPC-2. J Antimicrob Chemother, in press doi:10.1093/jac/dkz026.

24. Papp-Wallace KM, Winkler ML, Taracila MA, Bonomo RA. 2015. Variants of β-lactamase KPC-2 that are resistant to inhibition by avibactam. Antimicrob Agents Chemother 59:3710-7.

25. Calvopiña K, Hinchliffe P, Brem J, Heesom KJ, Johnson S, Cain R, Lohans CT, Fishwick CWG, Schofield CJ, Spencer J, Avison MB. 2017. Structural/mechanistic insights into the efficacy of nonclassical β-lactamase inhibitors against extensively drug resistant Stenotrophomonas maltophilia clinical isolates. Mol Microbiol 106:492-504.

26. Levitt PS, Papp-Wallace KM, Taracila MA, Hujer AM, Winkler ML, Smith KM, Xu Y, Harris ME, Bonomo RA. 2012. Exploring the role of a conserved class A residue in the Ω-Loop of KPC-2 β-lactamase: a mechanism for ceftazidime hydrolysis. J Biol Chem 287:31783-93.

27. Haidar G, Clancy CJ, Chen L, Samanta P, Shields RK, Kreiswirth BN, Nguyen MH. 2017. Identifying Spectra of Activity and Therapeutic Niches for Ceftazidime-Avibactam and Imipenem-Relebactam against Carbapenem-Resistant Enterobacteriaceae. Antimicrob Agents Chemother 61:e00642-17.

28. Shields RK, Clancy CJ, Hao B, Chen L, Press EG, Iovine NM, Kreiswirth BN, Nguyen MH. 2015. Effects of Klebsiella pneumoniae carbapenemase subtypes, extended-spectrum beta-lactamases, and porin mutations on the in vitro activity of

ceftazidime-avibactam against carbapenem-resistant K. pneumoniae. Antimicrob Agents Chemother 59:5793-7.

29. Forage RG, Lin EC. 1982. DHA system mediating aerobic and anaerobic dissimilation of glycerol in Klebsiella pneumoniae NCIB 418. J Bacteriol 151:591-9.

30. Mojica MF, Papp-Wallace KM, Taracila MA, Barnes MD, Rutter JD, Jacobs MR, LiPuma JJ, Walsh TJ, Vila AJ, Bonomo RA. 2017. Avibactam Restores the Susceptibility of Clinical Isolates of Stenotrophomonas maltophilia to Aztreonam. Antimicrob Agents Chemother 61:e00777-17.

31. Wolter DJ, Kurpiel PM, Woodford N, Palepou MF, Goering RV, Hanson ND. 2009. Phenotypic and enzymatic comparative analysis of the novel KPC variant KPC-5 and its evolutionary variants, KPC-2 and KPC-4. Antimicrob Agents Chemother 53:557-62.

32. Dixon M. 1953. The determination of enzyme inhibitor constants. Biochem J 55:170-1.

33. Barnes MD, Bethel CR, Alsop J, Becka SA, Rutter JD, Papp-Wallace KM, Bonomo RA. 2018. Inactivation of the Pseudomonas-Derived Cephalosporinase-3 (PDC-3) by Relebactam. Antimicrob Agents Chemother 62:e02406-17.

34. Krishnan NP, Nguyen NQ, Papp-Wallace KM, Bonomo RA, van den Akker F. 2015. Inhibition of Klebsiella β-Lactamases (SHV-1 and KPC-2) by Avibactam: A Structural Study. PLoS One 10:e0136813.

35. Majiduddin FK, Palzkill T. 2005. Amino acid residues that contribute to substrate specificity of class A beta-lactamase SME-1. Antimicrob Agents Chemother 49:3421-7.

837 36. Stewart NK, Smith CA, Frase H, Black DJ, Vakulenko SB. 2015. Kinetic and
838 structural requirements for carbapenemase activity in GES-type β-lactamases.
839 Biochemistry 54:588-97.
840 37. Doucet N, De Wals PY, Pelletier JN. 2004. Site-saturation mutagenesis of Tyr-105
841 reveals its importance in substrate stabilization and discrimination in TEM-1 beta-
842 lactamase. J Biol Chem 279:46295-303.
843 38. Doucet N, Pelletier JN. 2007. Simulated annealing exploration of an active-site
844 tyrosine in TEM-1 beta-lactamase suggests the existence of alternate conformations.
845 Proteins 69:340-8.
846 39. Papp-Wallace KM, Taracila M, Wallace CJ, Hujer KM, Bethel CR, Hornick JM,
847 Bonomo RA. 2010. Elucidating the role of Trp105 in the KPC-2 β-lactamase. Protein
848 Sci 19:1714-27.
849 40. Pemberton OA, Zhang X, Chen Y. 2017. Molecular Basis of Substrate Recognition
850 and Product Release by the Klebsiella pneumoniae Carbapenemase (KPC-2). J Med
851 Chem 60:3525-3530.
852 41. Petrella S, Ziental-Gelus N, Mayer C, Renard M, Jarlier V, Sougakoff W. 2008.
853 Genetic and structural insights into the dissemination potential of the extremely
854 broad-spectrum class A beta-lactamase KPC-2 identified in an Escherichia coli strain
855 and an Enterobacter cloacae strain isolated from the same patient in France.
856 Antimicrob Agents Chemother 52:3725-36.
857 42. Ke W, Bethel CR, Thomson JM, Bonomo RA, van den Akker F. 2007. Crystal
858 structure of KPC-2: insights into carbapenemase activity in class A beta-lactamases.
859 Biochemistry 46:5732-40.

860 43. King DT, King AM, Lal SM, Wright GD, Strynadka NC. 2015. Molecular
861 Mechanism of Avibactam-Mediated β-Lactamase Inhibition. ACS Infect Dis 1:175-
862 84.
863 44. Ourghanlian C, Soroka D, Arthur M. 2017. Inhibition by Avibactam and Clavulanate
864 of the beta-Lactamases KPC-2 and CTX-M-15 Harboring the Substitution N(132)G in
865 the Conserved SDN Motif. Antimicrob Agents Chemother 61:e02510-16.
866 45. Takebayashi Y, Wan Nur Ismah WAK, Findlay J., Heesom KJ, Zhang J, Williams
867 OM, MacGowan AP, Avison MB. 2017. Prediction Of Cephalosporin And
868 Carbapenem Susceptibility In Multi-Drug Resistant Gram-Negative Bacteria Using
869 Liquid Chromatography-Tandem Mass Spectrometry
870 doi:https://doi.org/10.1101/138594. bioRxiv
871 46. Gould VC, Okazaki A, Avison MB. 2006. Beta-lactam resistance and beta-lactamase
872 expression in clinical Stenotrophomonas maltophilia isolates having defined
873 phylogenetic relationships. J Antimicrob Chemother 57:199-203.
874 47. CLSI. 2015. M100-S25 performance standards for antimicrobial susceptibility testing;
875 Twenty-fifth informational supplement.
876 48. Cahill ST, Cain R, Wang DY, Lohans CT, Wareham DW, Oswin HP, Mohammed J,
877 Spencer J, Fishwick CW, McDonough MA, Schofield CJ, Brem J. 2017. Cyclic
878 Boronates Inhibit All Classes of β-Lactamases. Antimicrob Agents Chemother
879 61:e02260-16.
880 49. Winter G, Waterman DG, Parkhurst JM, Brewster AS, Gildea RJ, Gerstel M, Fuentes-
881 Montero L, Vollmar M, Michels-Clark T, Young ID, Sauter NK, Evans G. 2018.
882 DIALS: implementation and evaluation of a new integration package. Acta
883 Crystallogr D Struct Biol 74:85-97.

884 50. Winter G, Lobley CM, Prince SM. 2013. Decision making in xia2. Acta Crystallogr D
885 Biol Crystallogr 69:1260-73.
886 51. Collaborative Computational Project N. The CCP4 suite: programs for protein
887 crystallography.
888 52. McCoy AJ, Grosse-Kunstleve RW, Adams PD, Winn MD, Storoni LC, Read RJ.
889 2007. Phaser crystallographic software. J Appl Crystallogr 40:658-674.
890 53. Murshudov GN, Vagin AA, Dodson EJ. 1997. Refinement of macromolecular
891 structures by the maximum-likelihood method. Acta Crystallogr D Biol Crystallogr
892 53:240-55.
893 54. Adams PD, Afonine PV, Bunkoczi G, Chen VB, Davis IW, Echols N, Headd JJ,
894 Hung LW, Kapral GJ, Grosse-Kunstleve RW, McCoy AJ, Moriarty NW, Oeffner R,
895 Read RJ, Richardson DC, Richardson JS, Terwilliger TC, Zwart PH. 2010. PHENIX:
896 a comprehensive Python-based system for macromolecular structure solution. Acta
897 Crystallogr D Biol Crystallogr 66:213-21.
898 55. Emsley P, Cowtan K. 2004. Coot: model-building tools for molecular graphics. Acta
899 Crystallogr D Biol Crystallogr 60:2126-32.
900 56. Schrödinger L. The PyMOL Molecular Graphics System, vol Version 1.8.
901 57. O'Callaghan CH, Morris A, Kirby SM, Shingler AH. 1972. Novel method for
902 detection of beta-lactamases by using a chromogenic cephalosporin substrate.
903 Antimicrob Agents Chemother 1:283-8.
904 58. Xu H, Hazra S, Blanchard JS. 2012. NXL104 irreversibly inhibits the beta-lactamase
905 from Mycobacterium tuberculosis. Biochemistry 51:4551-7.
906 59. Mangat CS, Vadlamani G, Holicek V, Chu M, Larmour VLC, Vocadlo DJ, Mulvey
907 MR, Mark BL. 2019. Molecular Basis for the Potent Inhibition of the Emerging
908 Carbapenemase VCC-1 by Avibactam. Antimicrob Agents Chemother 63:02112-18.

60. Shapiro AB, Gao N, Jahic H, Carter NM, Chen A, Miller AA. 2017. Reversibility of Covalent, Broad-Spectrum Serine beta-Lactamase Inhibition by the Diazabicyclooctenone ETX2514. ACS Infect Dis 3:833-844.

61. Morrison JF, Walsh CT. 1988. The behavior and significance of slow-binding enzyme inhibitors. Adv Enzymol Relat Areas Mol Biol 61:201-301.

62. Jin W, Wachino JI, Yamaguchi Y, Kimura K, Kumar A, Yamada M, Morinaka A, Sakamaki Y, Yonezawa M, Kurosaki H, Arakawa Y. 2017. Structural Insights into the TLA-3 Extended-Spectrum β-Lactamase and Its Inhibition by Avibactam and OP0595. Antimicrob Agents Chemother 61:e00501-17.

63. Papp-Wallace KM, Winkler ML, Gatta JA, Taracila MA, Chilakala S, Xu Y, Johnson JK, Bonomo RA. 2014. Reclaiming the efficacy of β-lactam-β-lactamase inhibitor combinations: avibactam restores the susceptibility of CMY-2-producing Escherichia coli to ceftazidime. Antimicrob Agents Chemother 58:4290-7.

64. Poirel L, Ortiz De La Rosa JM, Kieffer N, Dubois V, Jayol A, Nordmann P. 2018. Acquisition of Extended-Spectrum β-Lactamase GES-6 Leading to Resistance to Ceftolozane-Tazobactam Combination in Pseudomonas aeruginosa. Antimicrob Agents Chemother 63:e01809-18.

65. Ruggiero M, Papp-Wallace KM, Taracila MA, Mojica MF, Bethel CR, Rudin SD, Zeiser ET, Gutkind G, Bonomo RA, Power P. 2017. Exploring the Landscape of Diazabicyclooctane (DBO) Inhibition: Avibactam Inactivation of PER-2 β-Lactamase. Antimicrob Agents Chemother 61:e02476-16.

932

Table 1. Minimal Inhibitory Concentrations of β-lactams Against *S. maltophilia* or *K. pneumoniae* in the Presence of β-lactamase Inhibitors.

	Ceftazidime		Imipenem		Aztreonam	
	-	+AVI (4 mg/L)	-	+REL (4 mg/L)	-	+REL (4 mg/L)
S. maltophilia K279a	16	8	128	64	>256	8
Ecl8 pUBYT	<0.125	-	<0.0625	-	-	-
Ecl8 pUBYT KPC-2	16	0.125	64	0.5	-	-
Ecl8 pUBYT KPC-3	128	<0.125	16	<0.125	-	-
Ecl8 pUBYT KPC-4	128	1	0.5	0.125	-	-

AVI, avibactam; REL, relebactam

933
934

Table 2. IC_{50} Values for DBO Inhibitors Against Class A β-Lactamases.

Protein	Avibactam (nM)	Relebactam (nM)
CTX-M-15	3.4 (0.02)	400 (0.04)
L2	15 (0.02)	470 (0.03)
KPC-2	10 (0.05)	230 (0.03)
KPC-3	29 (0.03)	260 (0.05)
KPC-4	9.3 (0.08)	910 (0.03)

Standard error of log IC_{50} values are shown in parentheses.

935
936

Table 3. Kinetic Parameters for Relebactam Inhibition.

	K_{iapp} (μM)	k_2/K ($M^{-1} s^{-1}$)	k_{off} (s^{-1})	t ½ (min)
L2	2.7 (0.7)	4000 (620)	0.00055 (0.000021)	21
CTX-M-15	21.0 (1.0)	540 (19)	0.00038 (0.000053)	30
KPC-2	1.2 (0.05)	4500 (220)	0.00087 (0.000032)	13
KPC-3	1.5 (0.05)	2100 (140)	0.00020 (0.000035)	58
KPC-4	4.8 (0.7)	1100 (190)	0.00019 (0.000038)	61

Errors in parentheses represent standard deviation (K_{iapp} and k_2/K) or standard error from fits of (k_{off}) from measurements carried out in triplicate.

937

938

Antimicrobial Agents and Chemotherapy

Table 4: Observed and Calculated Masses of KPC Variants Before and After Modification due to DBO Treatment. All differences between measured and expected masses are within experimental error. [a]Masses implied from maximum entropy deconvolution of measured spectra. [b]Masses were calculated based on protein sequences without an N-terminal methionine. [c]Corresponding to the observed protein masses. [d]'Acyl' denotes a mass shift corresponding to reaction of an intact DBO molecule.

		Mass(es) observed[a] [Da]	Mass calculated[b] [Da]	Mass shift(s) observed[c] [Da]	Mass shift calculated [Da]	Assignment[d*]
KPC2		30640	30640			
	+ avibactam	30905	30905	+ 265	+ 265	'acyl'
		30826	30825	+ 186	+ 185	'acyl' – 80
		30808	30807	+ 168	+ 167	'acyl' – 98
	+ relebactam	30989	30988	+ 349	+ 348	'acyl'
		30907	30908	+ 267	+ 268	'acyl' – 80
		30890	30890	+ 250	+ 250	'acyl' – 98
KPC3		30665	30667			
	+ avibactam	30931	30932	+ 266	+ 265	'acyl'
		30851	30852	+ 186	+ 185	'acyl' – 80
		30834	30834	+ 167	+ 167	'acyl' – 98
	+ relebactam	31013	31015	+ 348	+ 348	'acyl'
		30935	30935	+ 270	+ 268	'acyl' – 80
		30914	30917	+ 249	+ 250	'acyl' – 98
KPC4		30657	30657			
	+ avibactam	30922	30922	+ 265	+ 265	'acyl'
		30841	30842	+ 184	+ 185	'acyl' – 80
		30824	30824	+ 167	+ 167	'acyl' – 98
	+ relebactam	31005	31005	+ 348	+ 348	'acyl'
		30924	30925	+ 267	+ 268	'acyl' – 80
		30908	30907	+ 251	+ 250	'acyl' – 98

A chemical scheme depicting the assigned 'acyl', 'acyl' -80 and 'acyl' -98 species is displayed in **Figure 5A.*

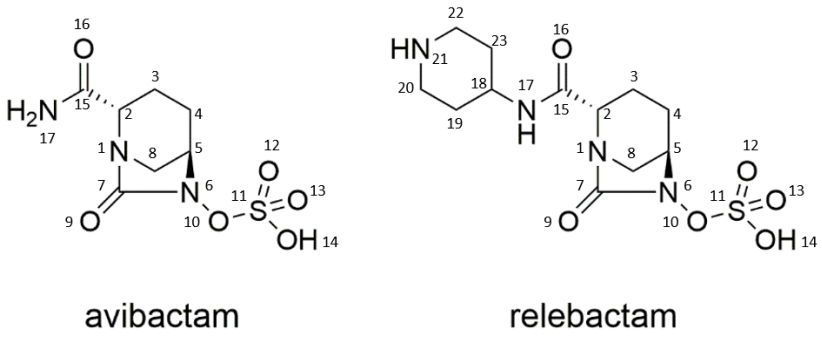

948
949
950 **Figure 1. Structures of the Diazabicyclooctanes (DBOs) Avibactam and Relebactam.**
951
952

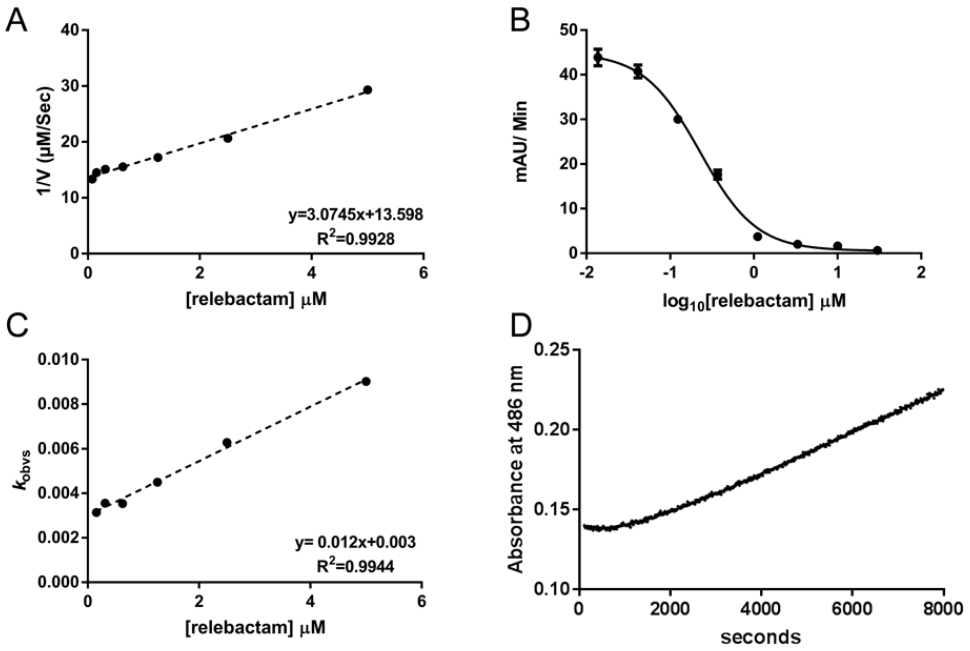

Figure 2. Kinetic Characterization of Relebactam Inhibition of KPC-2. (A) Dixon plot of reciprocals of initial nitrocefin hydrolysis rates (1/V) by enzyme:relebactam mixtures plotted against relebactam concentration. The apparent inhibition constant K_{iapp} is obtained from the slope of the fitted straight line. (B) Initial rates of nitrocefin hydrolysis (absorbance units/min) after 10-minute incubation with relebactam, plotted against $\log_{10}$ [relebactam]. Fitted curve is used to derive IC_{50} according to Equation 1. (C) Plot of k_{obs} (pseudo-first-order rate constant for inactivation) against relebactam concentration. The apparent second-order rate constant for the onset of carbamylation k_2/K is obtained from the slope of the fitted straight line. (D) Progress curve representing recovery of nitrocefin hydrolysis following 10 minute pre-incubation of enzyme (1 µM) with 17.5 µM relebactam, diluted to a final concentration of 50 nM enzyme. The rate of recovery of free enzyme, k_{off}**,** is obtained from the fitted line shown according to Equation 6. Data points shown are means of three replicate runs.

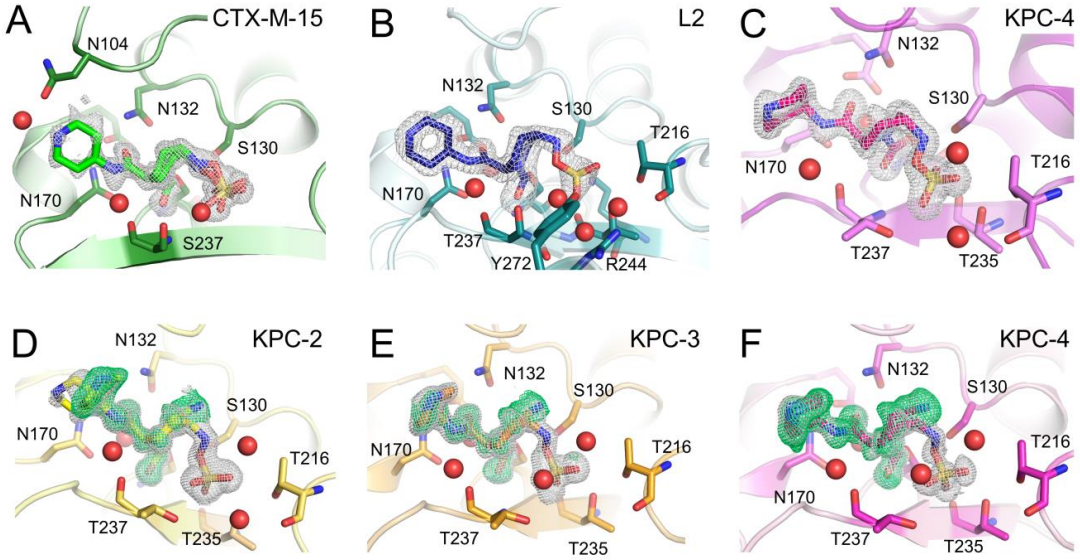

968

969 **Figure 3. Electron Density Maps Showing Relebactam Bound to the Active Sites of**
970 **Class A β-Lactamases.** Unbiased omit F_o-F_c electron density maps were calculated with the
971 ligand removed and are shown contoured at 3σ. Gray density is calculated after removal of
972 'intact' relebactam, green density after removal of desulfated relebactam. (A) CTX-M-15
973 (green, 16-hour soak); (B) L2 (teal, 16 hours); (C) KPC-4 (pink, 1 hour); (D) KPC-2 (yellow,
974 16 hours); (E) KPC-3 (orange, 16 hours); (F) KPC-4 (16 hours).
975

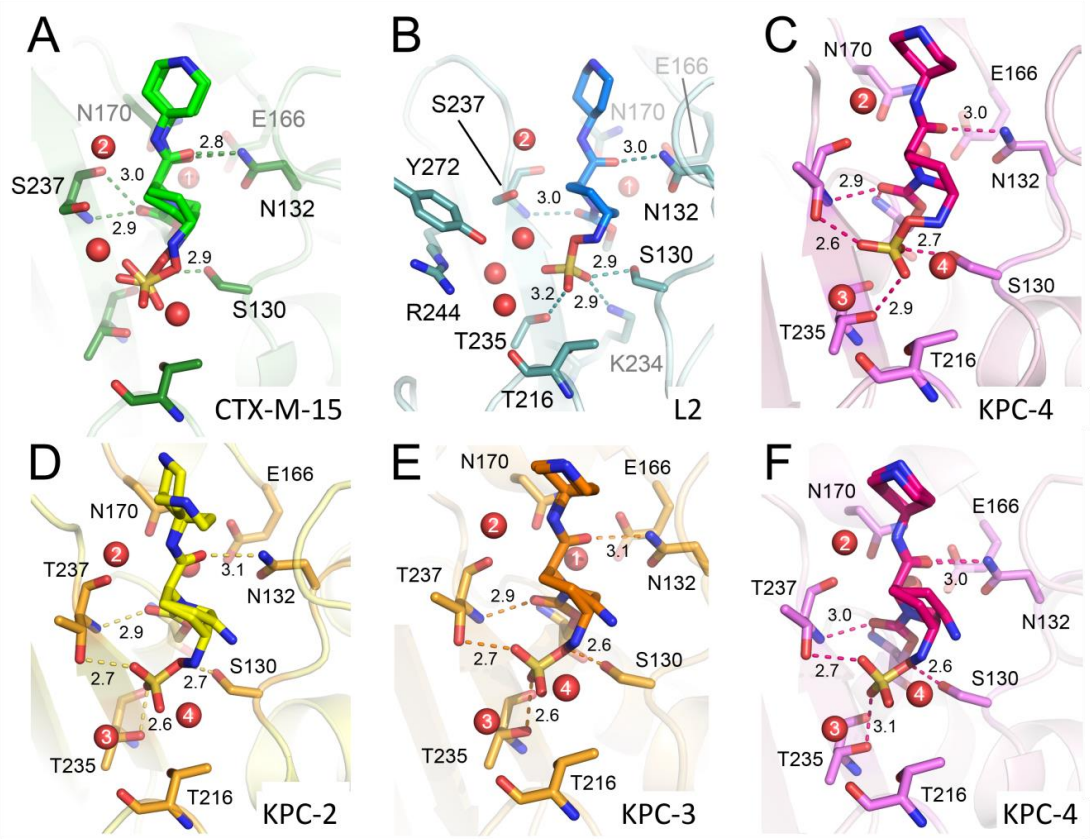

976 **Figure 4. Interactions of Relebactam with Active Sites of Class A β-Lactamases.** Close-
977 up views of relebactam bound in the active sites of class A β-lactamases (colored as in
978 **Figure 3**). Hydrogen bonding interactions of relebactam with the protein main chain are
979 shown as dashes with distances in Å. Water molecules are shown as red spheres; those that
980 make conserved interactions are numbered. (A) CTX-M-15 (16-hour soak) showing
981 relebactam bound in two conformations; (B) L2 (16-hour soak); (C) KPC-4 (1-hour soak).
982 Relebactam was modelled as both the imine (desulfated, 'acyl' -98 as shown in **Figure 5A**)
983 and 'intact' forms from 16-hour soaks of (D) KPC-2, (E) KPC-3 and (F) KPC-4 crystals.
984

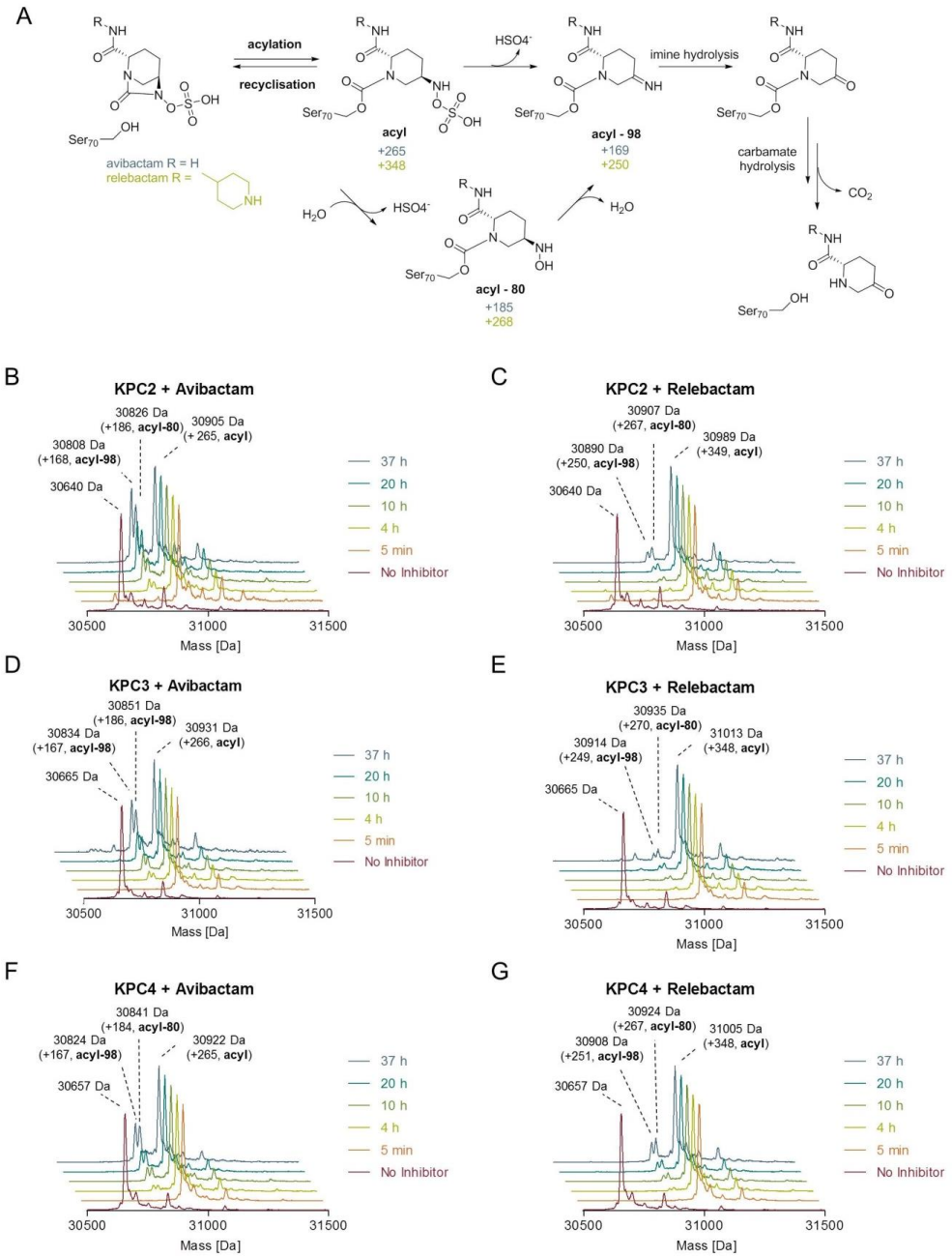

Figure 5: Time-Dependent Fragmentation of Covalent Avibactam and Relebactam Adducts. A) Chemical structures of proposed intermediates upon carbamylation and fragmentation pathways. B)-G) Deconvoluted ESI-MS spectra showing covalent modifications of KPC variants (KPC-2 -4) by DBOs over time. Enzymes were incubated with 2 equivalents of avibactam or relebactam in 50 mM Tris-HCl pH 7.5 at room temperature. Data are shown after maximum entropy deconvolution (MassHunter Qualitative Analysis software V.7 (Agilent Technologies)) over the mass range 1200-2000 Da.